Time-Resolved Transcriptomics Reveal Spliceosomal Disruption and Senescence Pathways in Crocin-Treated Hepatocellular Carcinoma Cells

David Roy Nelson[1,2,*], Amphun Chaiboonchoe[1,†], Weiqi Fu[1,‡], Amnah Salem Alzahmi[1,2], Ala'a Al-Hrout[3,§], Amr Amin[3,4,5,*], Kourosh Salehi-Ashtiani[1, 2,*]

[1]Division of Science, New York University Abu Dhabi, P.O. Box 129188, Abu Dhabi, UAE
[2]Center for Genomics and Systems Biology (CGSB), New York University Research Institute, New York University Abu Dhabi, P.O. Box 129188, Abu Dhabi, UAE
[3]College of Medicine, University of Sharjah, P.O. Box 27272, Sharjah, UAE
[4]The Summer Program, The University of Chicago, Chicago, IL 60637, USA
[5]College of Science, UAE University, P.O. Box 15551, Al Ain, UAE

*Corresponding to: ksa3@nyu.edu, a.amin@sharjah.ac.ae, and drn2@nyu.edu

[†] Present address - Siriraj Center of Research Excellence for Precision Medicine and Systems Pharmacology, Department of Pharmacology, Faculty of Medicine, Siriraj Hospital, Mahidol University, Bangkok, Thailand
[‡] Present address – State Key Laboratory of Ocean Sensing & Ocean College, Zhejiang University, Zhoushan, 316021, China
[§] Present address – IFOM ETS – The AIRC Institute of Molecular Oncology, Milan, Italy

Highlights:

- Time series transcriptomics reveals dynamic cellular responses to crocin treatment in HCC cells.
- Crocin induces significant downregulation of spliceosomal machinery across all time points.
- Crocin suppresses pro-proliferative pathways and activates tumor-suppressive mechanisms in HCC cells.
- Novel insights into crocin's anti-cancer effects provide potential new targets for HCC therapy.

Abstract: Natural products like saffron show promise in treating hepatocellular carcinoma (HCC), but their mechanisms remain unclear. Here, we used time-series transcriptomics to elucidate crocin's anti-cancer mechanisms in HCC cells. We treated HepG2 cells with 1 and 2 mM crocin for 2, 6, 12, and 24 hours and analyzed transcriptomic profiles at each timepoint. The strongest transcriptional response occurred at 2 hours with 1 mM crocin, with diminishing effects at later timepoints. We observed upregulation of metabolic-, adhesion-, and endocytosis-related genes across all timepoints. Pathway analysis revealed activation of DNA damage checkpoints and senescence while proliferation pathways were suppressed. Notably, 52 genes involved in non-alcoholic fatty liver disease were downregulated at 24 hours (FDR $p = 8 \times 10^{-8}$), suggesting reversal of carcinogenic pathways. Strikingly, crocin consistently downregulated spliceosomal machinery genes across all timepoints while upregulating senescence and autophagy pathways. This spliceosome targeting represents a clinically relevant mechanism, as aberrant splicing drives oncogenesis in more than 90% of cancers. The transcription factor PAX5 was significantly upregulated while oncogenic ELK1 targets were downregulated. Our findings show that crocin treatment is accompanied by HCC cell senescence induction through coordinated spliceosome disruption and metabolic reprogramming, providing novel therapeutic targets for hepatocellular carcinoma.

Keywords: Hepatocellular carcinoma (HCC), crocin, transcriptomics, spliceosome, senescence, natural anti-cancer compounds

---

1. Introduction

Saffron (*Crocus sativus L.*) and its bioactive component crocin have demonstrated anti-cancer properties in multiple studies, yet their molecular mechanisms remain incompletely understood. Crocin, a digentiobiose ester of crocetin, suppresses HCC cell survival through various downstream effectors [1]. We previously demonstrated that saffron extract exhibits pro-apoptotic, anti-inflammatory, and anti-oxidative effects against HCC both in vitro and in vivo [2].

Hepatocellular carcinoma represents the most common primary liver malignancy and a leading cause of cancer mortality worldwide [3]. Major risk factors include chronic hepatitis B/C infection, alcoholic liver disease, and non-alcoholic steatohepatitis (NASH), with 70-90% of patients having underlying chronic liver disease [4]. Current treatments include surgical resection, transplantation, and transarterial chemoembolization, but novel targeted therapies are urgently needed [5].

In this study, we used time-series transcriptomics to characterize the temporal dynamics of crocin's effects on HCC cells. We hypothesized that crocin induces time-dependent transcriptional changes that suppress cancer-promoting pathways while activating tumor-suppressive mechanisms. Our objectives were to: (1) characterize temporal transcriptomic changes following crocin treatment, (2) identify affected pathways and cellular processes, (3) elucidate mechanisms underlying crocin's anti-cancer effects, and (4) identify novel therapeutic targets for HCC.

2. Results

2.1. Time-series transcriptomics reveals dynamic cellular response to crocin

We performed comprehensive transcriptomic analysis of HepG2 cells treated with crocin at multiple timepoints (2, 6, 12, and 24 hours post-treatment (hpt)) using two concentrations (1 and 2 mM, corresponding to CR1 and CR2 treatments). The analysis employed transcription factor motif enrichment, gene ontology (GO) enrichment, and pathway analysis to characterize the cellular response.

Our results revealed a complex, time-dependent response characterized by rapid and sustained downregulation of spliceosomal machinery, activation of senescence and autophagy programs, and suppression of proliferative pathways (Fig. 1). This temporal pattern contrasts with recent single-cell RNA-seq findings by Guo et al. (2024), who identified persistent TOP2A+ proliferation phenotypes in HCC that maintain high expression levels over extended periods [6], suggesting that crocin uniquely disrupts this proliferative stability. The most pronounced transcriptional changes occurred at 2 hpt with 1 mM crocin, with the effect size diminishing at later timepoints and higher dose, suggesting an acute response that transitions to adaptation.

2.2. Transcription factor analysis reveals chromatin remodeling and cell fate changes

Transcription factor motif enrichment analysis of differentially expressed genes revealed distinct regulatory patterns (Fig. 1). Genes containing promoter motifs for SP1/2, RREB1, PLAG1, PAX5, OSR1, EGR1, and ELF1 were rapidly upregulated following treatment, indicating these factors mediate the early transcriptional response. Notably, ELK1 target genes showed decreased expression at 2 and 6 hpt. As ELK1 regulates redox homeostasis through glutathione metabolism [7], crocin's antioxidant properties likely disrupt this oncogenic pathway. PAX5 binding motifs were highly enriched in upregulated genes at 6, 12, and 24 hpt. Given PAX5's role in chromatin remodeling [8], this suggests that crocin modulates epigenetic states to influence cell fate decisions.

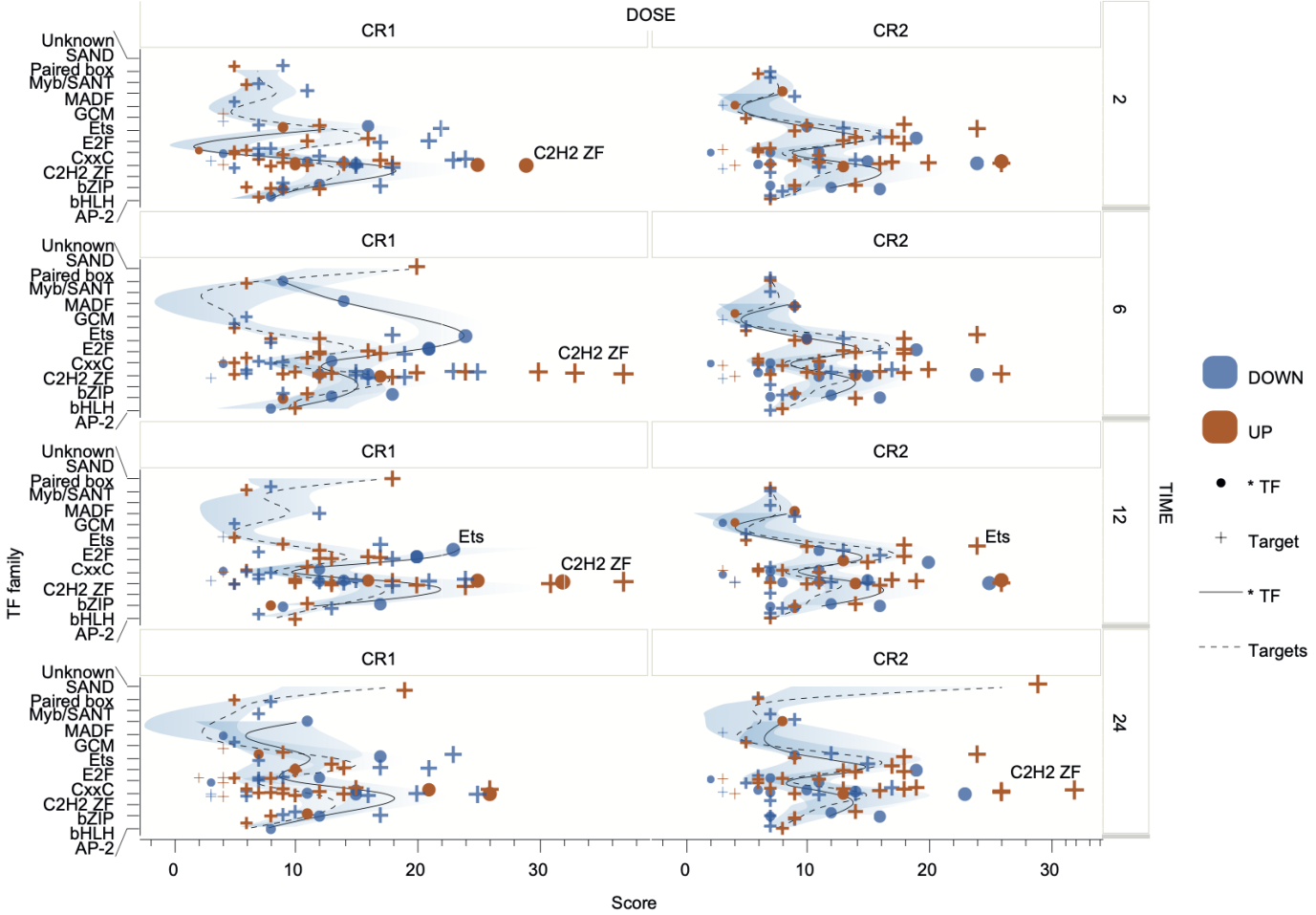

Figure 1. Transcription factor (TF) motif enrichment in differentially expressed genes (DEGs) following crocin treatment of HCC cells. The graph displays enrichment in upregulated (empty circles) and downregulated (blue circles) DEGs, with polynomial fits for distribution comparisons. Genes containing promoter motifs for TFs SP, SP2, RREB1, PLAG1, PAX5, OSR1, EGR1, and ELF1 were rapidly upregulated post-treatment, suggesting their involvement in the cellular response to crocin. The C2H2 zinc finger TF family binding motifs were prominently represented in dysregulated genes, consistent with their diverse roles in cellular function and cancer [9]. This analysis provides insights into the transcriptional regulatory networks affected by crocin in HCC cells, highlighting potential mechanisms of its anti-cancer effects.

2.3. Crocin induces progressive downregulation of spliceosomal machinery

A striking finding was the consistent downregulation of spliceosomal components across all timepoints (Fig. 2). At 2 hours, four key genes were affected: SRSF2, RBM39, PRPF6, and SNRPC, targeting both core components and regulatory factors. By 6 hpt, this expanded to 16 splicing-related genes, including additional SR proteins (SRSF7, SRSF8), their kinase SRPK1, and mRNA export factors (ALYREF, DDX39A).

This temporal progression from focused to broad spliceosome disruption suggests initial targeting of key regulatory nodes followed by comprehensive machinery dysfunction. At 24 hpt, while some early changes persisted, new genes emerged (DDX39B, TXNL4A) and RNA degradation factors (EXOSC7) were affected, indicating establishment of a new RNA processing steady state.

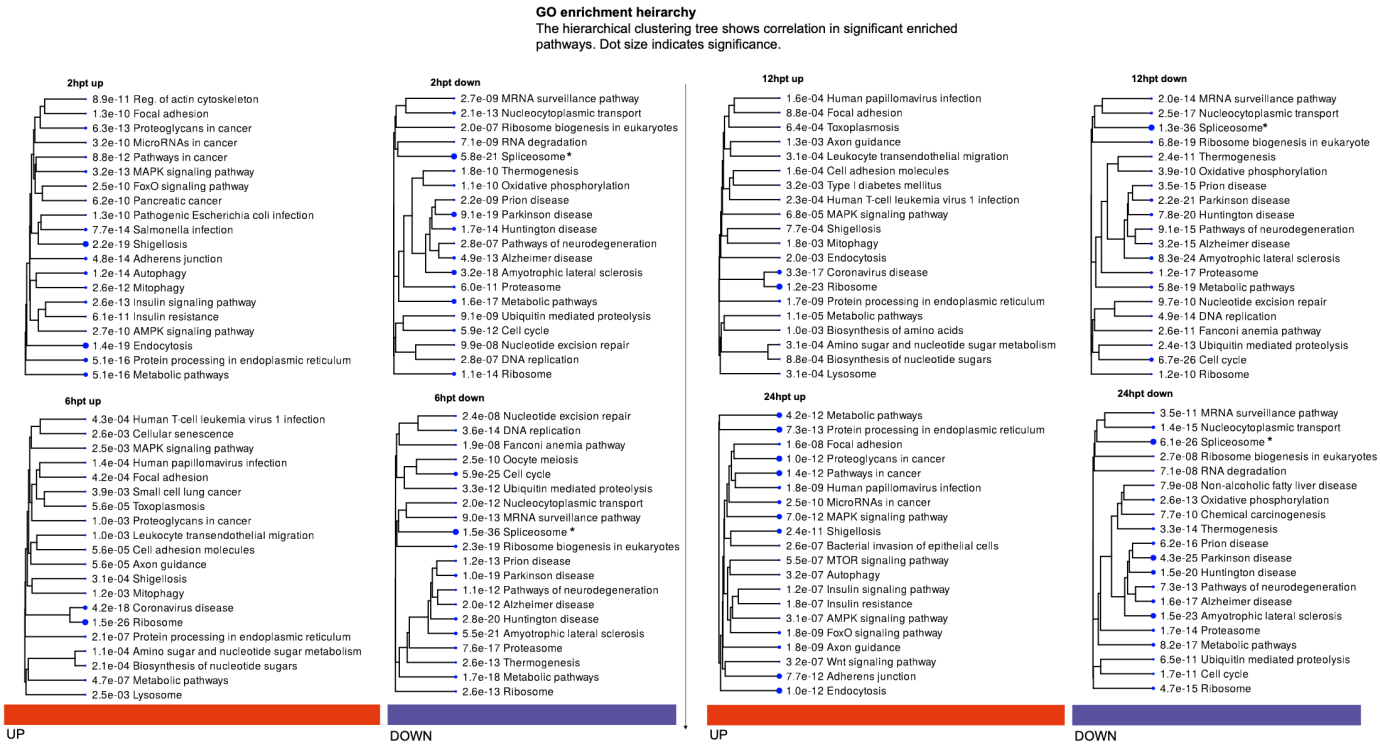

Figure 2. Gene ontology (GO) enrichment hierarchies for up- and down-regulated DEGs after crocin treatment in HCC cells. Genes constituting the shown GO terms are significantly dysregulated after crocin treatment (FDR $p < 0.05$), but the processes represented by the GO terminology are not necessarily involved. Dysregulated genes involved in several other disease processes are referred to by the mentioned GO terms, but it is only their shared, overlapping gene sets that were analyzed. Transcriptomes from 2,6,12, and 24 hpt of crocin-exposed HCC cells revealed consistent decreases in spliceosomal machinery expression and processes involved in cell cycle progression. In contrast, MAPK, AMPK, MTOR, and microRNA signaling pathways were upregulated.

2.4. Activation of autophagy and senescence programs

Crocin treatment significantly upregulated autophagy genes (ATG12, ULK3, MALT1, MAPK3) and senescence markers (CDKN2A/p16, BRD4) beginning at 2 hpt. This dual activation likely results from multiple mechanisms: oxidative stress activating MAPK3/ULK3, ER stress triggering ATG12, and DNA damage promoting CDKN2A/BRD4 expression.

2.5. Pathway analysis reveals senescence induction without apoptosis

Gene Ontology analysis revealed time-dependent shifts in cellular processes (Fig. 2). Early responses (2 to 6 hpt) showed metabolic changes, while later timepoints (12-24 hpt) featured sustained autophagy and endocytosis upregulation alongside continued spliceosome suppression. We further investigated changes 24 hpt with Ingenuity Pathway Analysis for further detail into pathway-level effects.

At 24 hpt, we identified five pathways with major perturbations: 'Molecular mechanisms of cancer', 'Axonal guidance signaling', 'Protein ubiquitination', 'Aldosterone signaling', and 'Unfolded protein response'. Surprisingly, apoptosis was inhibited (Fig. 3), with CHOP-mediated BCL2 activation and ASK1-MKK7-JNK1 downregulation, suggesting senescence and an anti-inflammatory response (Fig. 4), rather than apoptosis, drives crocin's effects.

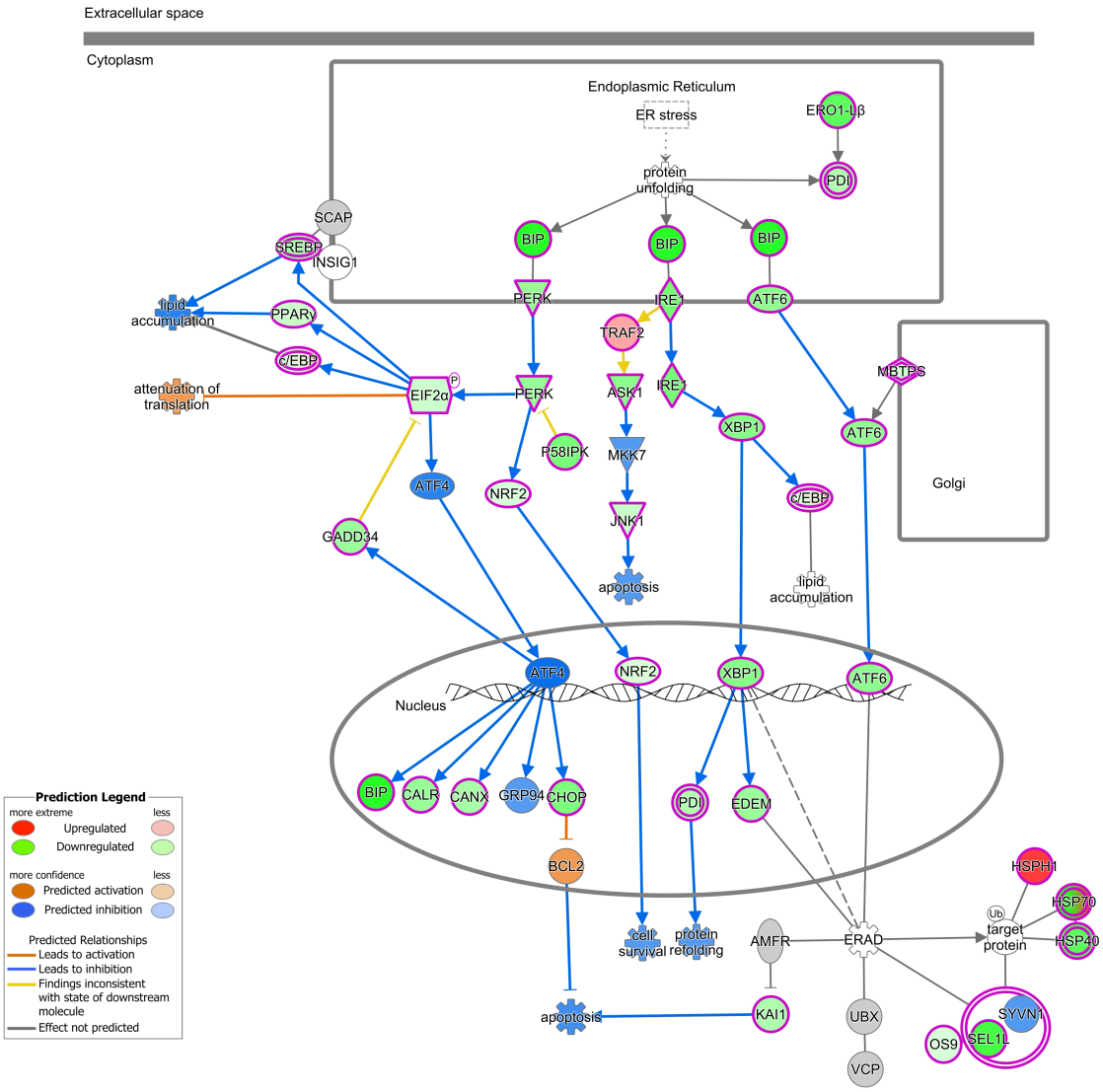

Figure 3. Apoptotic pathway analysis showing inhibition at 24 hpt. RNA-Seq data analysis using the Ingenuity Molecule Activity Predictor (MAP) in IPA revealed inhibition and activation patterns in the apoptotic pathway. Gene expression is represented by color, with red indicating upregulation and green indicating downregulation. The intensity of color corresponds to the magnitude of $\log_2$ - fold change change. Processes are color-coded based on their predicted activation state, with orange representing activation and blue representing inhibition. Edges connecting nodes are colored to represent regulatory effects: orange for activating effects of upstream regulators on target processes, blue for inhibitory effects, and yellow for inconsistencies with predictions based on previous findings. Key observations in the figure include CHOP activation of BCL2 leading to apoptosis inhibition, and down-regulation of the ASK1 - MKK7 - JNK1 apoptotic pathway. These findings suggest that crocin's mechanism for inhibiting proliferation may not be solely attributed to apoptosis induction. Results from the 2 hpt timepoint offer an alternative explanation: cells may be entering senescence and producing signals that attract immune cells for their destruction.

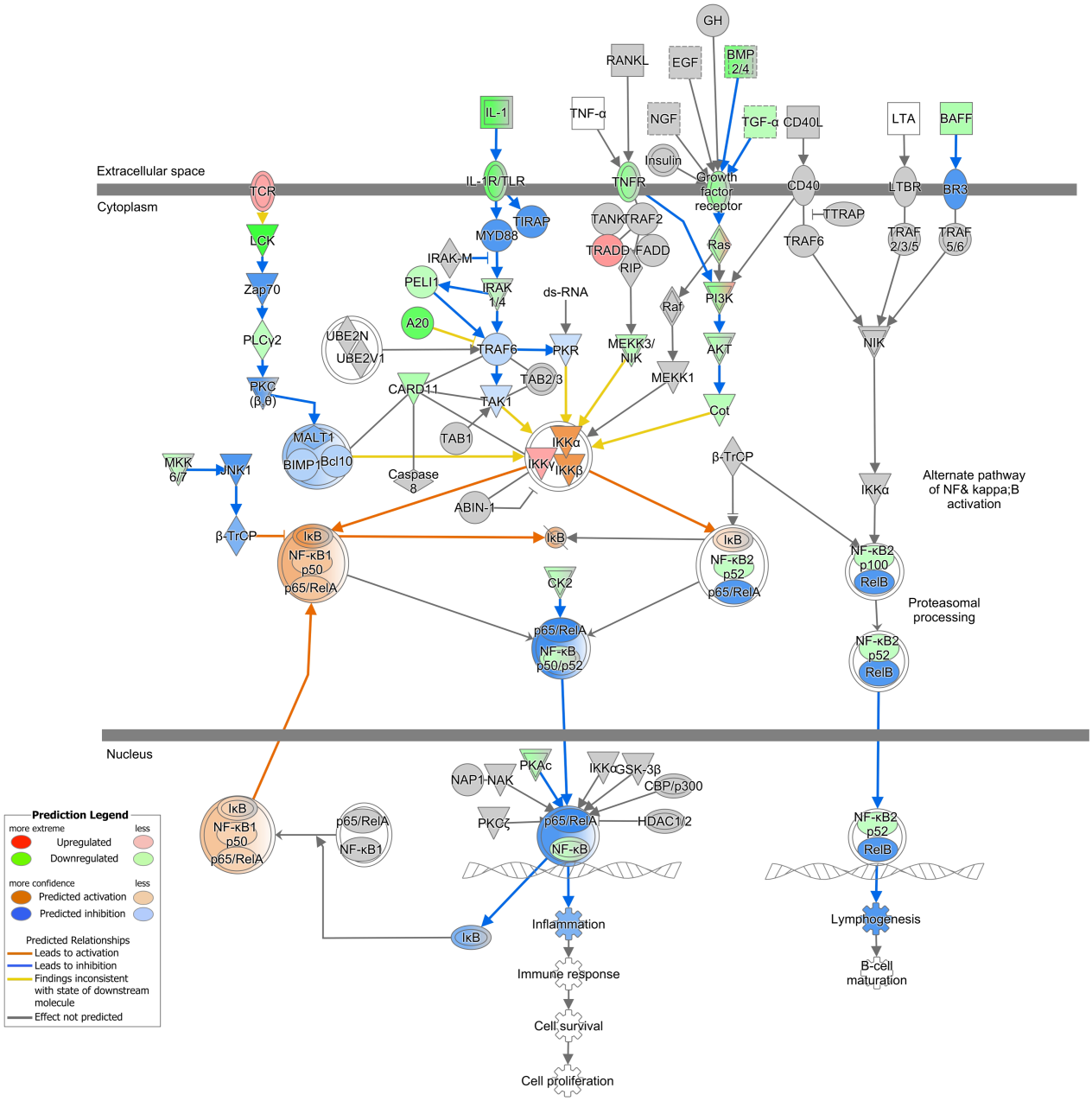

Fig. 4. NF-κB signaling pathway showing anti-inflammatory response. We used the Ingenuity Molecule Activity Predictor (MAP) to predict the upstream and downstream effects of the mapped genes in this pathway. Colored nodes and their intensity indicate genes that were up-regulated (red) or down-regulated (green) from the input datasets. Orange and blue nodes indicate genes predicted to be activated or inhibited after 24 hpt' crocin treatment, respectively. Edges between nodes are colored orange, blue, yellow and gray, signifying activation, inhibition, inconsistent and not predicted, respectively. Abbreviations of gene names are according to standard abbreviations used in GenBank. Here, NF-kB activation is predicted to be lessened by crocin treatment, leading to a downregulation of inflammation pathways. Notably, 52 genes involved in non-alcoholic fatty liver disease were downregulated at 24 hpt (FDR $p = 8 \times 10^{-8}$), indicating reversal of carcinogenic pathways.

3. Discussion

Our time-series analysis reveals novel mechanisms underlying crocin's anti-cancer effects, most notably the consistent downregulation of spliceosomal machinery. This finding is particularly significant as splicing dysregulation drives oncogenesis in >90% of cancers [10], and FDA-approved spliceosome modulators show efficacy in hematologic malignancies [11]. While spliceosome dysregulation in HCC has been documented, our findings reveal a unique temporal pattern of disruption. Unlike the competing endogenous RNA networks described that maintain splicing homeostasis in HCC [12,13], crocin systematically dismantles this machinery, suggesting a novel therapeutic vulnerability.

The magnitude of changes we observed contrasts sharply with normal HepG2 behavior in culture, where gene expression typically varies by less than 3-fold and proliferative pathways remain highly active [14]. The temporal progression from early metabolic changes to later senescence/autophagy activation provides mechanistic insight. Early fatty acid oxidation and cholesterol metabolism changes likely reflect acute stress responses. The subsequent shift toward senescence—evidenced by CDKN2A upregulation and proliferation pathway suppression—represents a potent

tumor-suppressive mechanism [15]. Senescent cells undergo irreversible growth arrest and can trigger immune-mediated clearance. In contrast to the high expression of cell cycle and proliferation genes typically observed in untreated HepG2 cells [14], crocin treatment suppressed these pathways, with proliferation markers significantly downregulated by 24 hpt.

The dual activation of autophagy and senescence, without apoptosis induction, distinguishes crocin's mechanism from conventional cytotoxic agents. Autophagy may initially serve as a survival response but can lead to cell death when hyperactivated [16,17]. The NF-κB pathway downregulation further supports an anti-proliferative, pro-senescence phenotype.

4. Conclusions

Our analyses reveal that crocin induces HCC cell senescence through coordinated disruption of spliceosomal machinery and metabolic reprogramming. The discovery of spliceosome targeting as a primary mechanism provides a novel therapeutic avenue for HCC treatment. Combined with senescence induction and autophagy activation, these findings explain crocin's multi-faceted anti-cancer effects and suggest potential for combination therapies targeting these pathways.

Future studies should validate these findings at the protein level and *in vivo* models, explore specific splice variants affected, and investigate combination strategies leveraging crocin's unique mechanisms.

5. Materials and Methods

5.1 HCC Cell culture

The liver cancer cell line HepG2 was cultured in RPMI 1640 medium (HyClone, Logan, UT, USA) supplemented with 10% fetal bovine serum (Sigma-Aldrich, Burlington, MA, USA) containing 1% of antibiotic/ antimycotic solution (Grand Island Biological Company (GIBCO); Thermo-Fisher Scientific, Waltham, MA, USA). Cells were incubated at 37 °C in a humidified 5% CO_2 atmosphere, and sub-cultured every 3-5 days using 0.25% trypsin (HyClone, Logan, UT, USA).

5.2 Crocin treatment

HepG2 cells were incubated with 1 mM (CR1) or 2 mM (CR2) of crocin (Sigma-Aldrich, Burlington, MA, USA) for 2, 6, 12, and 24 hour time courses. Cells were trypsinized and pelleted. Cell pellets were resuspended in RNAlater stabilization solution (Ambion, from Invitrogen by Thermo Fischer Scientific, Carlsbad, California, USA) and stored in -80 ºC. All experiments were carried out in triplicates. Six untreated samples were taken at time point 0 and constitute the controls. Thus, an important limitation of this study is the lack of time-matched controls for time points beyond 0 hpt. To address potential limitations arising from our sampling experimental design, we employed the following strategies. First, we focused on large-magnitude changes: We prioritized discussion of gene expression changes that were substantial and unlikely to be solely due to natural fluctuations in culture. The finding of the largest effect size at 2 hpt indicated a substantial impact on cellular processes from crocin. Where possible, we compared our observed changes to published data on HCC cell behavior in culture over similar periods. Published data shows that untreated HepG2 cells maintain relatively stable transcriptomic profiles in culture, with technical replicates showing correlations of $r > 0.99$ and most genes varying less than two-fold [14]. The dramatic changes we observed, including widespread spliceosomal downregulation and metabolic reprogramming, clearly exceed normal culture-related variations, supporting our focus on large-magnitude changes. These approaches allowed us to mitigate the potential confounding effects of natural changes in gene expression over time in cultured cells, effects of cell cycle progression, and potential stress responses due to prolonged culture conditions.

5.3 RNAseq libraries construction and sequencing

Total RNA was isolated from three biological replicates of crocin-treated and untreated samples using an RNeasy Mini Kit (Qiagen, Hilden, DE) following the manufacturer's instructions. The RNAseq libraries were prepared using TruSeq RNA sample prep kit (Illumina, Inc., San Diego, CA, USA) following the manufacturer's instructions. Briefly, TruSeq RNA sample prep kit converts the poly-A containing mRNA in total RNA into a cDNA library using poly-T oligo-attached magnetic bead selection. Following mRNA purification, the RNA is chemically fragmented prior to reverse transcription and cDNA generation. The fragmentation step yields an RNAseq library that includes inserts ranging in size from approximately 100-400 bp. The average insert size in an Illumina TruSeq RNA sequencing library is approximately 200 bp. The cDNA fragments then go through an end repair process, the addition of a single 'A' base to the 3' end followed by ligation of the adapters. Then, the products are purified and enriched with PCR to create the final double-stranded cDNA libraries. Finally, library quality control and quantification were performed using a Bioanalyzer Chip DNA 1000 series II (Agilent, Santa Clara, CA, USA) and sequenced directly using the high-throughput Illumina HiSeq sequencing system (Illumina, Inc., San Diego, CA, USA).

5.4 Alignment and analysis of Illumina reads against the reference genome

Paired End (PE) reads from each library (crocin treatments with selected time points and in addition to the control sample) were generated using CASAVA version 1.8.2 package in Fastq format. The Trimmomatic[18,19] package was used to remove adapters and filter out low quality bases (Q < 20). Filtered sequences reads were mapped to the ENSEMBL[20] human genome sequence (ENSEMBL-release-81-GRCh38), which was used as a reference to align the transcriptome reads. To characterize gene expression in cells, FPKM values (Fragments Per Kilobase of transcript per Million mapped reads) were calculated and used as a normalized measure of read density that allows transcript levels to be compared both within and between samples quantitatively. The algorithms DESeq2 [21] and Kallisto [22] were used to identify differentially expressed genes (DEGs) between two groups of samples (triplicates within each group). Specifically, DESeq2 was used in a pipeline to generate the IPA results and Kallisto was used for all other analyses.

5.5 Ingenuity Pathway Analysis

We used the Ingenuity Pathway Analysis (IPA; Ingenuity Systems, Inc., Redwood City, CA, USA) to examine the biological network associated with changes in RNA expression levels from the crocin treatment at 12 and 24 hpt. The IPA software (http://www.ingenuity.com) uses a manually curated database which contains information from several sources, including published journal papers and gene annotation databases. Fisher's exact test was used to calculate the probabilities between the input gene set and the canonical pathways. We also used IPA to predict the upstream and downstream effects of activation or inhibition on other molecules based on the input gene set's expression data.

5.6 GO analyses

All query genes are first converted to ENSEMBL {Dyer, 2025 #49} gene IDs or STRING-db {Szklarczyk, 2025 #50} protein IDs. Our gene ID mapping and pathway data were derived from these two sources and processed using ShinyGO (https://bioinformatics.sdstate.edu/go/) {Ge, 2020 #51}. False discovery rate (FDR) was calculated based on the nominal P-value from the hypergeometric test. Fold-enrichment was defined as the percentage of genes in the list belonging to a pathway, divided by the corresponding percentage in the background. Due to increased statistical power, large pathways tend to have smaller FDRs. As a measure of effect size, fold-enrichment indicates the degree of overrepresentation of genes in a pathway. Only pathways that are within the specified size limits are used for enrichment analysis. After the analysis is done, pathways are first filtered based on a user-specified FDR cutoff. Then the significant pathways were sorted by FDR, fold-enrichment, or other metrics. We first selected the top pathways by FDR, then sorted these by fold enrichment. Similar pathways sharing 95% of their genes were represented instead by the single most significant pathway. Redundant pathways also needed to share 50% of the words in their names.

5.7 Statistical Analysis

Statistical analyses were performed using JMP software (version 16.0 PRO, SAS Institute Inc., Cary, NC, USA). For continuous dependent variables and categorical independent variables, we conducted pairwise comparisons across all levels of the categorical variables. Each comparison included a standard t-test, a test of practical significance, and an equivalence test. We implemented an outlier detection method for each continuous dependent variable and categorical independent variable. Outliers were defined as points whose distance to the predicted value exceeded three times the estimated sigma (i.e., points with standardized residuals exceeding three). These outlier indicators were saved as new columns in the original data table, grouped under the 'outlier group' category. Robust fits and robust estimates were used for outlier detection, with the same three-sigma criterion applied. For both residual analysis and outlier detection, we performed robustness checks by repeating the analyses with the robust option selected.

Data Availability: All data used for these analyses are provided as supplementary materials for this manuscript to ensure reproducibility and facilitate further exploration of the results (Zenodo doi:10.5281/zenodo.12632036; https://zenodo.org/records/15804191). Sequencing reads are available at Zenodo doi: 10.5281/zenodo.13822023 (controls; https://zenodo.org/records/13822024) and doi:10.5281/zenodo.13842438 (crocin treatment time points 2, 6, 12, and 24 hpt; https://zenodo.org/records/13842439).

Author Contributions: D.R.N. and A.C. performed bioinformatic analysis and drafted the manuscript. W.F. and A.S.A. contributed to manuscript preparation and revision. A.A.H. and A.S.A. performed laboratory experiments. A.A. and K.S.A. secured funding, developed the experimental design, and provided overall project supervision. All authors reviewed and approved the final version of the manuscript.

Funding: This research was supported by NYUAD Faculty Research Funds (AD060), Tamkeen under the NYU Abu Dhabi Research Institute Award to the NYUAD Center for Genomics and Systems Biology (73 71210 CGSB9), and the University of Sharjah's Grant No. (24010901156).

Conflicts of Interest: The authors declare no conflicts of interest

Bibliography

1. Yao, C.; Liu, B.-B.; Qian, X.-D.; Li, L.-Q.; Cao, H.-B.; Guo, Q.-S.; Zhou, G.-F. Crocin induces autophagic apoptosis in hepatocellular carcinoma by inhibiting Akt/mTOR activity. *OncoTargets and therapy* **2018**, *11*, 2017.

2. Amin, A.; A Hamza, A.; Daoud, S.; Khazanehdari, K.; Al Hrout, A.; Baig, B.; Chaiboonchoe, A.; E Adrian, T.; Zaki, N.; Salehi-Ashtiani, K. Saffron-based crocin prevents early lesions of liver cancer: in vivo, in vitro and network analyses. *Recent patents on anti-cancer drug discovery* **2016**, *11*, 121-133.

3. Jindal, A.; Thadi, A.; Shailubhai, K. Hepatocellular carcinoma: etiology, current and future drugs. *Journal of Clinical and Experimental Hepatology* **2019**.

4. Zhu, R.X.; Seto, W.-K.; Lai, C.-L.; Yuen, M.-F. Epidemiology of hepatocellular carcinoma in the Asia-Pacific region. *Gut and liver* **2016**, *10*, 332.

5. Liu, C.-Y.; Chen, K.-F.; Chen, P.-J. Treatment of liver cancer. *Cold Spring Harbor perspectives in medicine* **2015**, *5*, a021535.

6. Guo, D.Z.; Zhang, X.; Zhang, S.Q.; Zhang, S.Y.; Zhang, X.Y.; Yan, J.Y.; Dong, S.Y.; Zhu, K.; Yang, X.R.; Fan, J.; et al. Single-cell tumor heterogeneity landscape of hepatocellular carcinoma: unraveling the pro-metastatic subtype and its interaction loop with fibroblasts. *Mol Cancer* **2024**, *23*, 157, doi:10.1186/s12943-024-02062-3.

7. Yang, B.; Wang, H.; Xiao, J.; Chen, W.; Chen, W. ELK1/KIFC1 axis promotes breast cancer cell proliferation by regulating glutathione metabolism. *J Obstet Gynaecol Res* **2023**, *49*, 2175-2184, doi:10.1111/jog.15710.

8. Cobaleda, C.; Schebesta, A.; Delogu, A.; Busslinger, M. Pax5: the guardian of B cell identity and function. *Nat Immunol* **2007**, *8*, 463-470, doi:10.1038/ni1454.

9. Jen, J.; Wang, Y.C. Zinc finger proteins in cancer progression. *J Biomed Sci* **2016**, *23*, 53, doi:10.1186/s12929-016-0269-9.

10. Urbanski, L.M.; Leclair, N.; Anczukow, O. Alternative-splicing defects in cancer: Splicing regulators and their downstream targets, guiding the way to novel cancer therapeutics. *Wiley Interdiscip Rev RNA* **2018**, *9*, e1476, doi:10.1002/wrna.1476.

11. Peng, Q.; Zhou, Y.; Oyang, L.; Wu, N.; Tang, Y.; Su, M.; Luo, X.; Wang, Y.; Sheng, X.; Ma, J.; et al. Impacts and mechanisms of alternative mRNA splicing in cancer metabolism, immune response, and therapeutics. *Mol Ther* **2022**, *30*, 1018-1035, doi:10.1016/j.ymthe.2021.11.010.

12. Tang, Z.; Li, X.; Zheng, Y.; Liu, J.; Liu, C.; Li, X. The role of competing endogenous RNA network in the development of hepatocellular carcinoma: potential therapeutic targets. *Front Cell Dev Biol* **2024**, *12*, 1341999, doi:10.3389/fcell.2024.1341999.

13. Niu, Z.S.; Wang, W.H.; Dong, X.N.; Tian, L.M. Role of long noncoding RNA-mediated competing endogenous RNA regulatory network in hepatocellular carcinoma. *World J Gastroenterol* **2020**, *26*, 4240-4260, doi:10.3748/wjg.v26.i29.4240.

14. Tyakht, A.V.; Ilina, E.N.; Alexeev, D.G.; Ischenko, D.S.; Gorbachev, A.Y.; Semashko, T.A.; Larin, A.K.; Selezneva, O.V.; Kostryukova, E.S.; Karalkin, P.A.; et al. RNA-Seq gene expression profiling of HepG2 cells: the influence of experimental factors and comparison with liver tissue. *BMC Genomics* **2014**, *15*, 1108, doi:10.1186/1471-2164-15-1108.

15. Faget, D.V.; Ren, Q.; Stewart, S.A. Unmasking senescence: context-dependent effects of SASP in cancer. *Nat Rev Cancer* **2019**, *19*, 439-453, doi:10.1038/s41568-019-0156-2.

16. Leidal, A.M.; Levine, B.; Debnath, J. Autophagy and the cell biology of age-related disease. *Nat Cell Biol* **2018**, *20*, 1338-1348, doi:10.1038/s41556-018-0235-8.

17. Mizushima, N.; Levine, B. Autophagy in Human Diseases. *N Engl J Med* **2020**, *383*, 1564-1576, doi:10.1056/NEJMra2022774.

18. Sewe, S.O.; Silva, G.; Sicat, P.; Seal, S.E.; Visendi, P. Trimming and Validation of Illumina Short Reads Using Trimmomatic, Trinity Assembly, and Assessment of RNA-Seq Data. *Methods Mol Biol* **2022**, *2443*, 211-232, doi:10.1007/978-1-0716-2067-0_11.

19. Bolger, A.M.; Lohse, M.; Usadel, B. Trimmomatic: a flexible trimmer for Illumina sequence data. *Bioinformatics* **2014**, *30*, 2114-2120, doi:10.1093/bioinformatics/btu170.

20. Dyer, S.C.; Austine-Orimoloye, O.; Azov, A.G.; Barba, M.; Barnes, I.; Barrera-Enriquez, V.P.; Becker, A.; Bennett, R.; Beracochea, M.; Berry, A.; et al. Ensembl 2025. *Nucleic Acids Res* **2025**, *53*, D948-D957, doi:10.1093/nar/gkae1071.

21. Love, M.I.; Anders, S.; Huber, W. Analyzing RNA-seq data with DESeq2. *R package reference manual* **2017**.

22. Bray, N.L.; Pimentel, H.; Melsted, P.; Pachter, L. Near-optimal probabilistic RNA-seq quantification. *Nat Biotechnol* **2016**, *34*, 525-527, doi:10.1038/nbt.3519.